Acta Pharmaceutica Sinica B 2025;15(10):5010−5021

Chinese Pharmaceutical Association
Institute of Materia Medica, Chinese Academy of Medical Sciences

Acta Pharmaceutica Sinica B

www.elsevier.com/locate/apsb
www.sciencedirect.com

ORIGINAL ARTICLE

Dissecting the effects of ^{223}Radium on the bone microenvironment

Sergio Barrios[a,b], Elisa Serafini[c,d], Ludovica La Posta[a], D. Nicole Meyers[e], Nicholas J. Dunbar[e], Paul G. Corn[a], Florent Elefteriou[f], Catherine G. Ambrose[e], Stefano Casarin[c,d,g], Antonios G. Mikos[b], Eleonora Dondossola[a,*]

[a]*David H. Koch Center and Genitourinary Medical Oncology Department, University of Texas MD Anderson Cancer Center, Houston, TX 77030, USA*
[b]*Department of Bioengineering, Rice University, Houston, TX 77030, USA*
[c]*Center for Precision Surgery, Houston Methodist Research Institute, Houston, TX 77030, USA*
[d]*LaSIE, UMR 7356 CNRS, La Rochelle Université, La Rochelle 17042, France*
[e]*Department of Orthopedic Surgery, University of Texas Health Science Center, Houston, TX 77030, USA*
[f]*Department of Orthopedic Surgery, Baylor College of Medicine, Houston, TX 77030, USA*
[g]*Department of Surgery, Houston Methodist Hospital, Houston, TX 77030, USA*

Received 6 January 2025; received in revised form 30 May 2025; accepted 4 June 2025

KEY WORDS

^{223}Radium;
Bone;
Bone microenvironment;
Radioisotope;
Osteoblast;
Osteoclast;
Zoledronic acid;
Alpha-emitter;
Fluorescence microscopy

Abstract Radium-223 (^{223}Ra) is a bone-seeking, alpha-particle-emitting radionuclide that is approved for the treatment of patients with metastatic prostate cancer and is currently being tested in clinical trials for primary and metastatic cancers to the bone. ^{223}Ra accumulates in mineralized bone areas with high bone turnover, where its effects are confined within 100 μm of the bone−marrow interface due to the short tissue penetrance of the alpha particles. A recent clinical study has shown a significantly increased fracture rate associated with the administration of ^{223}Ra, mostly in tumor-free bones. Importantly, the biological mechanisms underlying this bone fragility remain unclear. In this work, we combined micro-computed tomography and mechanical studies with *ex vivo* spatial biology analysis based on 3D fluorescence microscopy to clarify the effects of ^{223}Ra on bone and key bone stromal cell components. We found that ^{223}Ra caused major trabecular bone loss with no detectable impact on cortical bone. In addition, ^{223}Ra impaired osteoblast bone-forming activity, which was paralleled by a transient increase in osteoclast number and long-term adipocyte formation. Overall, these results suggest that the impact of

This article is part of a special issue entitled: Targeted Radiopharmaceuticals published in Acta Pharmaceutica Sinica B.

*Corresponding author.
E-mail address: EDondossola@mdanderson.org (Eleonora Dondossola).

Peer review under the responsibility of Chinese Pharmaceutical Association and Institute of Materia Medica, Chinese Academy of Medical Sciences.

https://doi.org/10.1016/j.apsb.2025.07.035

^{223}Ra on bone health is orchestrated by multiple bone stromal cell components. ^{223}Ra-mediated trabecular bone loss was prevented by administration of zoledronic acid, which should always be combined with ^{223}Ra.

1. Introduction

Prostate cancer (PCa) is a highly prevalent malignancy worldwide that exhibits a propensity for secondary growth in bone[1-3]. These secondary lesions induce skeletal-related complications, including pain, spinal cord compression, hypercalcemia, diminished mobility, and fractures[4,5], which have a negative impact on patient quality of life and survival[3].

Radium-223 (^{223}Ra) is an alkaline earth metal radioisotope with properties similar to calcium; upon administration, ^{223}Ra selectively binds to hydroxyapatite, which is highly enriched in the bone matrix[6]. This incorporation is more pronounced in areas of active bone remodeling, *e.g.*, at the front of the growth plate or in metastatic lesions[6]. ^{223}Ra emits alpha particles with high energy but limited tissue penetrance (<100 μm) [7], which minimizes its impact on healthy bone marrow tissue and reduces the side effects commonly associated with the use of β-emitters[6,8,9]. In men afflicted with metastatic PCa to bone, ^{223}Ra prolonged the median overall survival (3.6 months) and delayed the time to first symptomatic skeletal event (5.8 months) compared to placebo[7,10]. These results led to the approval of ^{223}Ra as the first bone-targeted radioligand for the treatment of metastatic PCa patients with symptomatic bone lesions and no visceral involvement[7,10]. Since then, ^{223}Ra has been clinically investigated for other cancer types that colonize the bone, including multiple myeloma, hormone-positive breast cancer, renal cell carcinoma, non-small cell lung cancer, and differentiated thyroid cancer[11-13].

The efficacy of ^{223}Ra in patients correlates with a sustained decline in osteoblast-derived alkaline phosphatase (ALP) in serum, denoting reduced bone turnover, which was not associated with increased bone fragility in the ALSYMPCA clinical trial[7]. A recent prospective clinical trial investigating the effects of ^{223}Ra on bone health by whole-body magnetic resonance imaging (MRI) showed a higher fracture rate, mostly asymptomatic, in patients receiving ^{223}Ra. Sixty-eight percent of the fractures occurred in bones without metastases[14], suggesting a systemic rather than tumor-dependent effect on bone biology. However, the mechanisms leading to ^{223}Ra-associated bone fragility remain unclear, and scarce and contrasting data are available on the effects of ^{223}Ra on bone stromal cells. *In vitro*, ^{223}Ra inhibits osteoblast and osteoclast differentiation (but not bone resorption) at doses >400 Bq/mL and induces their activation at doses <200 Bq/mL[11]. In mouse models of PCa bone metastasis, ^{223}Ra decreases the number of osteoblasts and osteoclasts in mice implanted with LNCaP, whereas in mice implanted with LuCap58, it only reduces the number of osteoblasts[15].

External beam radiation is often used in patients with bone tumors, and its effects on bone health are well documented[16-19]. External beam radiation in rodent models has been shown to induce bone marrow adipogenesis, impaired mechanical properties, altered material composition, increased osteoclastogenesis, trabecular bone loss, and cytotoxic effects on osteoblasts and bone-lining cells[20-23]. However, ^{223}Ra fundamentally differs from traditional external beam radiation, *i.e.*, alpha radiation is constantly emitted from the bone itself with a half-life of 11.4 days and a maximum penetrance of 100 μm[8]. Therefore, the impact of ^{223}Ra on bone health may differ substantially from that of external beam radiation.

Interestingly, ^{223}Ra-induced bone fragility can be mitigated through the administration of bone-protecting agents, such as zoledronic acid (ZA), as recently assessed in the EORTC-1333-GUCG trial[24]. Besides evidence of reduced osteoclast numbers via a decrease in TRACP5b circulating levels in tumor-bearing mice treated with ^{223}Ra and ZA, no further studies have been performed to address the mechanisms underlying such improvements in bone health. A more thorough evaluation of the radiobiological effects of ^{223}Ra on the bone matrix and cells is thus needed to support a meaningful and safe application of this agent in patients.

In this study, we evaluated the effects of ^{223}Ra treatment on the bone microenvironment. We combined 3D fluorescence microscopy, micro-computed tomography, mechanical testing, and computational simulations to investigate the impact of ^{223}Ra on bone, including its effects on bone mechanical properties and resident cell populations, as well as the impact of ZA in mitigating ^{223}Ra-induced bone damage.

2. Materials and methods

2.1. *In vivo studies*

Animal studies were approved by the Institutional Animal Care and Use Committee (IACUC) of the University of Texas MD Anderson Cancer Center and were performed according to the institutional guidelines for animal care and handling. Details are provided in the Supporting Information

2.2. *Statistical analysis*

Statistical analysis was performed using GraphPad Prism 10.0. Data are shown as mean ± standard deviation (SD). An unpaired two-sided Student's *t* test was applied to analyze two populations, whereas one-way ANOVA followed by the Tukey honestly significant difference (HSD) *post hoc* test, was performed to compare more than two populations. All statistical tests were two-sided, and *P* values less than 0.05 were considered statically significant. Further experimental methods are detailed in the Supporting Information

3. Results

3.1. *Effects of ^{223}Ra on bone microarchitecture*

To monitor the impact of ^{223}Ra on bone microarchitecture, we performed *ex vivo* micro-computed tomography (micro-CT) on

adult mouse tibiae (8 weeks old, $n = 4$/group) harvested at 1, 2, 4, 6, and 8 weeks after a single injection of ^{223}Ra (300 kBq/kg) or vehicle (normal saline) (Fig. 1A). Consistent with previous reports on radiation-induced trabecular bone damage[19], we observed trabecular bone microarchitecture destruction in the proximal tibia metaphysis region as early as 1 week post ^{223}Ra treatment (Fig. 1B and C). Specifically, ^{223}Ra treatment induced a significant decrease in bone volume fraction, bone surface, and bone mineral density compared to control. Furthermore, ^{223}Ra induced a significant increase in trabecular separation and decrease in trabecular number (Fig. 1B and C). These are both key markers of bone remodeling and reflect an altered state induced by ^{223}Ra. Tibiae collected 2 weeks post treatment showed further trabecular bone impairment, which stabilized 4 weeks post ^{223}Ra injection and remained stable up to 8 weeks post injection (Supporting Information Fig. S1). Cortical and trabecular bone thickness did not show significant differences at any timepoint. To confirm these findings in a different skeletal element, micro-CT analysis was performed on lumbar spine samples harvested at 4 weeks. Results showed similar trends, with a significant decrease in key trabecular bone parameters (Supporting Information Fig. S2). Taken together, these data show that ^{223}Ra impairs trabecular bone architecture but does not affect cortical bone.

3.2. *Effects of ^{223}Ra on bone mechanical properties*

To assess the consequences of ^{223}Ra on bone mechanical properties, we performed three-point bending test analysis on mouse femurs ($n = 5$ to 8/group). Femurs were harvested at 2, 4, and 8 weeks post ^{223}Ra (300 kBq/kg) or vehicle (saline) injection (Fig. 2A and B), and mechanical testing was performed. The stiffness and rigidity of the femurs were slightly, but significantly, increased for the ^{223}Ra group at 2 weeks as compared to control (Fig. 2C). The ultimate load, ultimate strength, elastic modulus, and cross-sectional area parameters did not show any significant differences (Fig. 2C). Taken together, these data suggest that ^{223}Ra treatment has very limited and transient effects on the mechanical properties of murine long bones. However, the three-point bending test mainly provides information on cortical bone mechanical properties (not trabecular bone), which were not expected to significantly change based on micro-CT analysis (see Fig. 1B and C). To investigate the mechanical properties of trabecular bone, we used tibial micro-CT trabecular bone data (2, 4 and 8 weeks) to develop a microstructural finite element analysis (m-FEA) of a central cubic volume (0.5 mm × 0.5 mm × 0.5 mm) of trabecular bone (Fig. 2D and E). m-FEA is a well-established method to study the mechanical behavior of trabecular bone under loading conditions[25-27]. By simulating a uniaxial compression test, m-FEA results predicted a significant, progressive decrease in stiffness and increased deformation for the ^{223}Ra-treated group compared to the control group at 4 and 8 weeks post treatment (Fig. 2D). A significant increase in both maximum Von Mises stress (a measure of the overall stress state of the material under compressive loading) and strain (a measure of the deformation of the material with respect to the applied load) was also observed in the ^{223}Ra-treated group compared to the control group at both 4 and 8 weeks (Fig. 2D). These results were further coupled with a significant rise in the maximum strain energy and in the ratio of total energy per number of trabeculae at both 4 and 8 weeks, in alignment with a reduced number of trabeculae (Fig. 2D). In addition, no

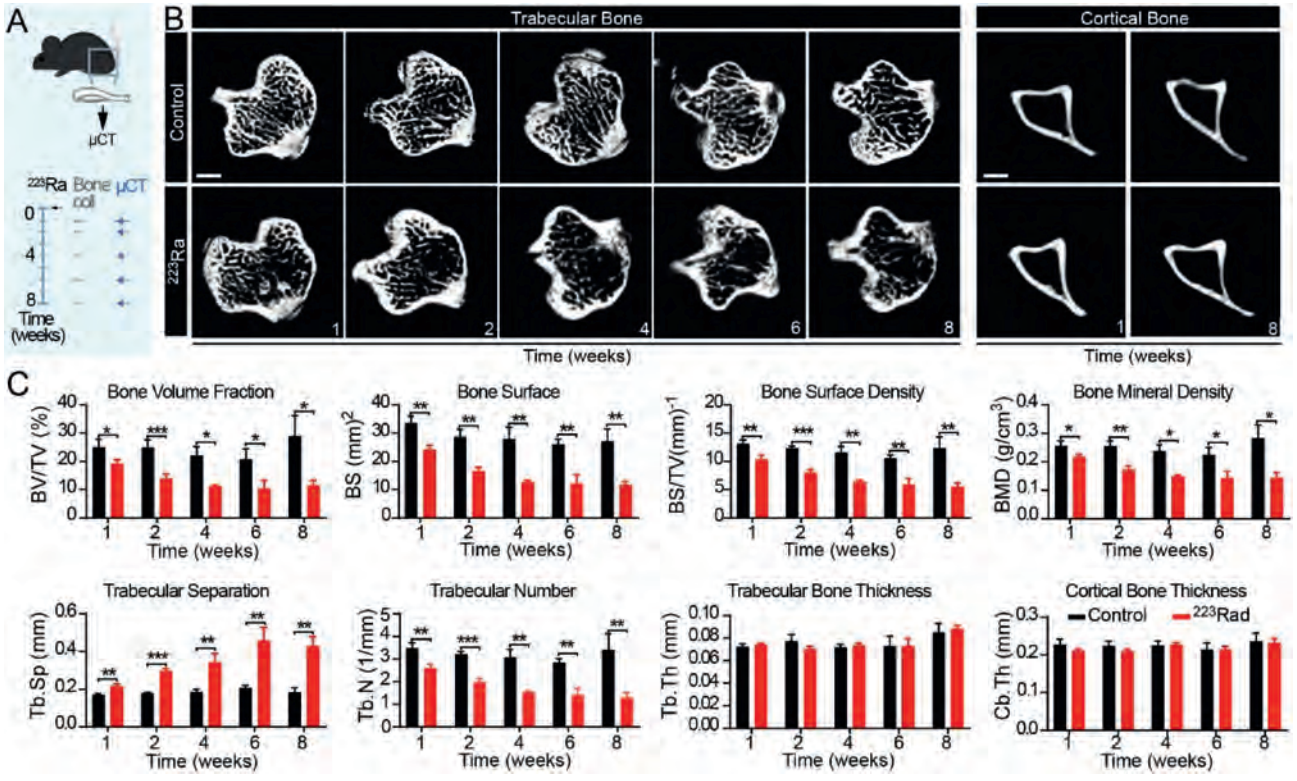

Figure 1 ^{223}Ra disrupts bone microarchitecture and mineral density. (A) Experimental design. (B) Representative micro-CT micrographs. Bar, 300 μm. (C) Micro-CT analysis of bone structural parameters. Bar, 300 μm. *P* values by unpaired two-tailed Student's *t* test, $P < 0.05$ (*); $P < 0.01$ (**); $P < 0.0001$ (***).

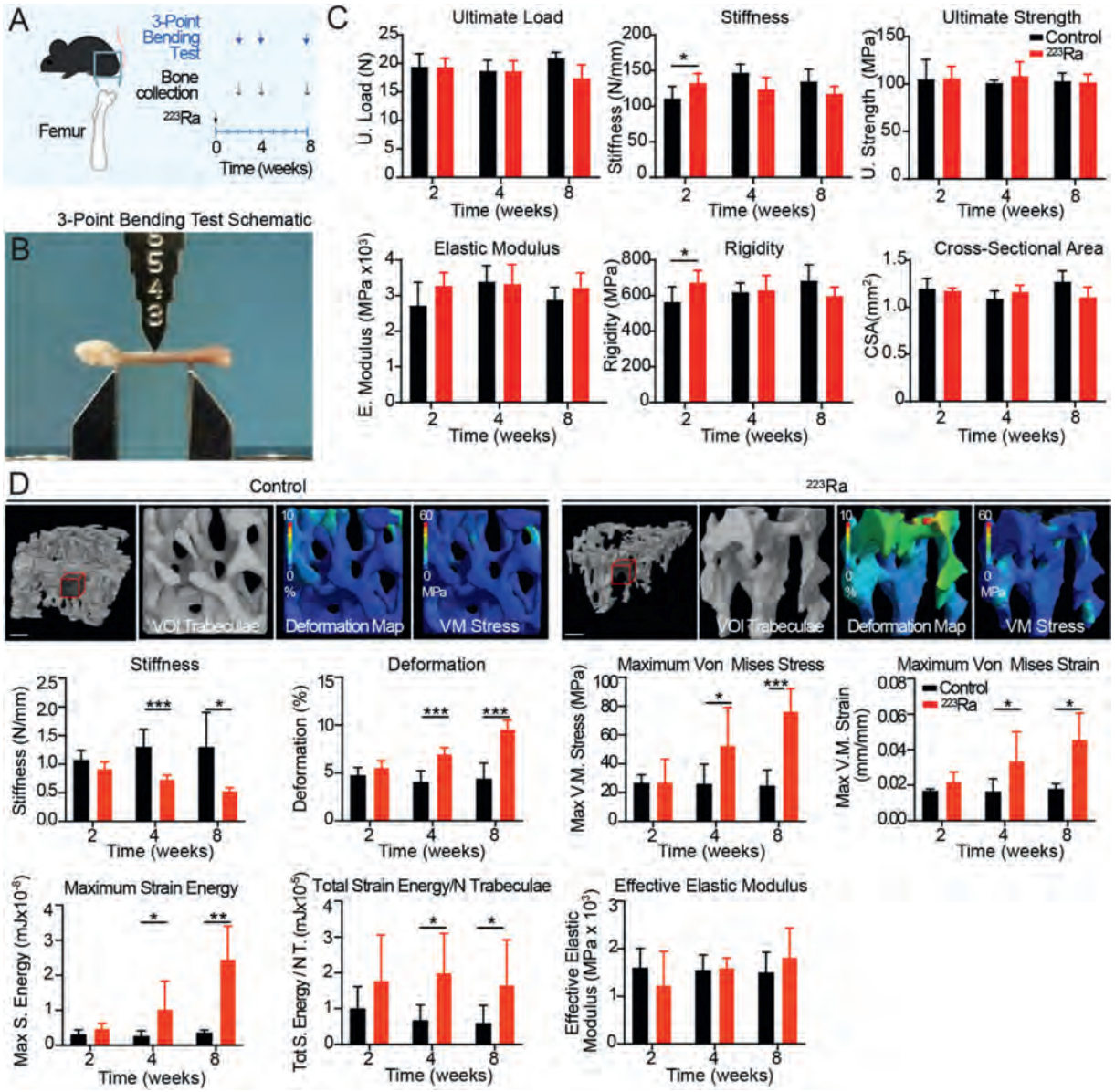

Figure 2 Effects of ^{223}Ra on bone mechanical properties. (A) Experimental design. (B, C) 3-point bending test setup and mechanical analysis. (D) m-FEA analysis; representative images (micro-CT-derived volume, deformation and Von Mises stress maps at 4 weeks) with quantifications are shown. Bar, 500 µm. *P* values by unpaired two-tailed Student's *t* test, $P < 0.05$ (*); $P < 0.01$ (**); $P < 0.001$ (***).

significant differences were observed in the effective elastic modulus, with values closely matching the initial micro-CT-derived elastic modulus ($E = 1695$ MPa). This is in line with the expectation that, within the linear elastic regime, stress and strain remain proportional and, consequently, their ratio also remains unchanged. Altogether, these results suggest that ^{223}Ra impacts the mechanical properties of trabecular bone but not of cortical bone.

To evaluate the impact of ^{223}Ra on trabecular bone composition, we performed confocal Raman microscopy on the condyle region of mouse femurs ($n = 7$ to 17 scans/group). For this purpose, bones were harvested at two timepoints (2 and 4 weeks) after a single injection of ^{223}Ra (300 kBq/kg) or vehicle (saline). Raman spectra analysis showed a significant increase in collagen crosslinking 4 weeks after ^{223}Ra treatment as compared to control. Interestingly, this increase was coupled with a significant decrease in collagen density at the same timepoint (Supporting Information Fig. S3). Taken together, confocal Raman analysis on femoral trabecular bone suggests a direct impact of ^{223}Ra on the degree of collagen crosslinking and collagen density in the bone matrix.

3.3. Direct impact of radiation vs. cell mediated effects of ^{223}Ra on bone microarchitecture

To determine whether the deleterious effects of ^{223}Ra on bone microarchitecture are predominantly caused by the direct impact of radiation on mineralized bone tissue or are mediated by the cells, mouse tibiae were harvested 2 days after a single injection of ^{223}Ra (300 kBq/kg) or vehicle (saline) (Supporting

Information Fig. S4A). To account for different preservation methods that could impact the effects of ^{223}Ra therapy, tibiae were either fixed with 70% ethanol and kept at 4 °C, or frozen and kept at −20 °C without fixation. *Ex vivo* micro-CT analysis was then performed at 1, 2, and 4 weeks after ^{223}Ra or vehicle injection. Contrary to our previous findings, bone micro-architecture was stable and did not show any significant changes in bone parameters across different timepoints regardless of the sample preservation method (Fig. S4B and S4C). Taken together, these micro-CT data suggest that the trabecular bone loss induced by ^{223}Ra does not simply rely on direct damage inflicted by bone-targeted alpha radiation but is largely cell mediated.

3.4. *Effects of ^{223}Ra on osteoblasts in vivo and in vitro*

To monitor the *in vivo* effects of ^{223}Ra on osteoblasts (bone-forming cells), we used a fluorescent reporter mouse model expressing mCherry fluorochrome under the control of the osterix (Osx) promoter. Osx, also called Sp7, is a cell-specific transcription factor expressed by mature osteoblasts and osteocytes that regulates their differentiation[28]. Sp7-mCherry mice were treated with ^{223}Ra (300 kBq/kg) or vehicle and euthanized at different timepoints up to 60 days. Tibiae were harvested, decalcified, and sectioned into thick slices (300 µm) using a vibratome. Slices from the tibial metaphysis region were stained with DAPI (nuclear

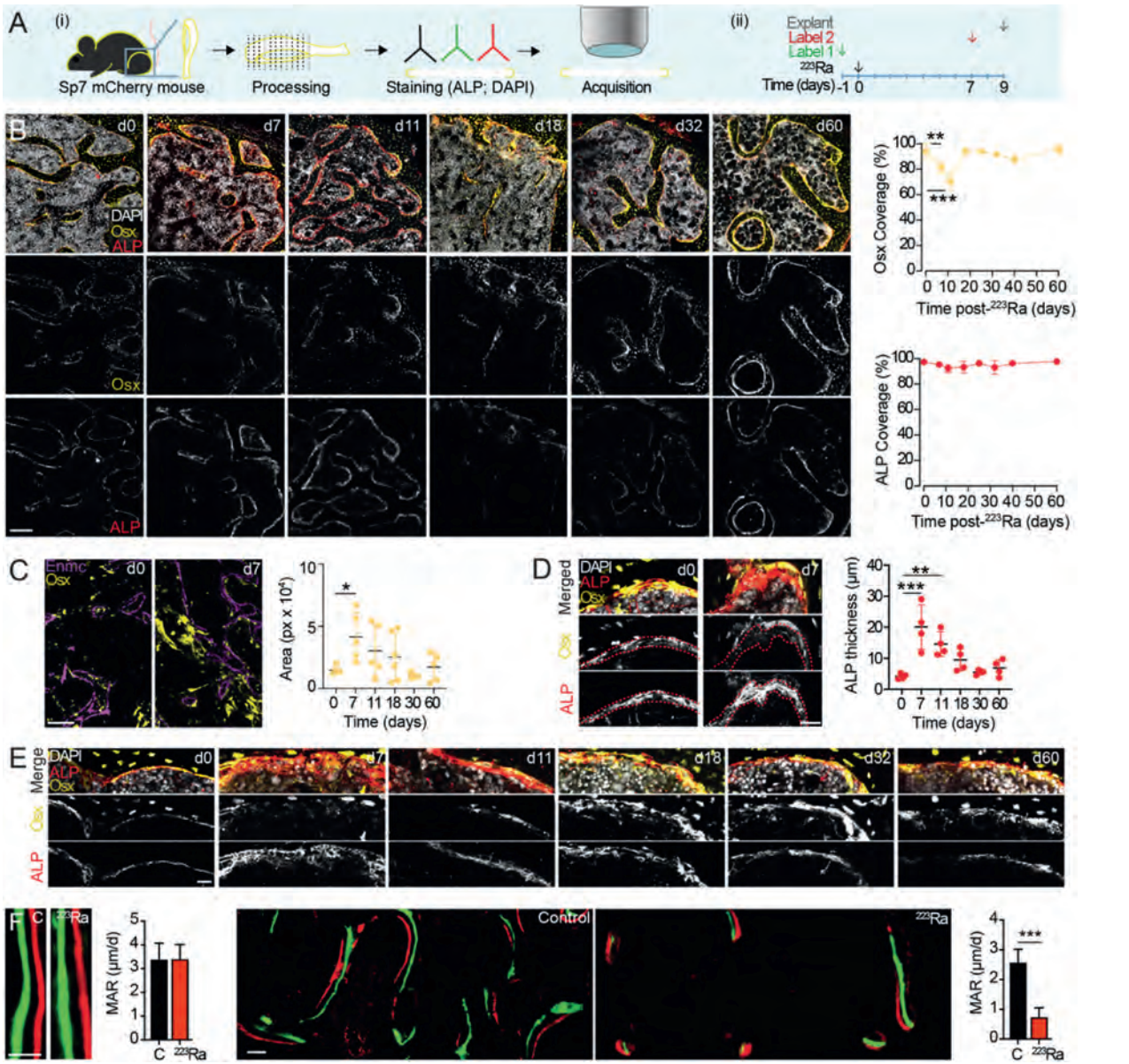

Figure 3 Effects of ^{223}Ra on osteoblasts *in vivo*. (A) Experimental design; (i) immunofluorescence; (ii) dual bone labelling. (B) Osx and ALP, representative images and quantification ($n = 5$) in tibiae at different timepoints post ^{223}Ra treatment. Bar, 100 µm. (C) Osx$^+$ cells into the bone marrow, representative images and quantifications. Bar, 50 µm. (D, E) ALP$^+$ layer thickness, representative images and quantification (altered co-localization of osx$^+$ cells is shown). Bar, 30 µm. (F) Representative images and quantification of mineral apposition of femoral sections (green, calcein green; red, xylenol orange; $n = 6$). Bar, 50 µm. *P* values by one-way ANOVA with Tukey's HSD *post hoc* test; $P < 0.05$ (*); $P < 0.01$ (**); $P < 0.001$ (***).

counterstain) and an anti-alkaline phosphatase (ALP) antibody (Fig. 3A). ALP, an early osteogenic marker of bone formation, is a membrane-associated glycoprotein that increases local concentrations of inorganic phosphate and facilitates bone mineralization[29]. Images were acquired via confocal microscopy, and image analysis was performed using FIJI[30] to quantify the impact of ^{223}Ra on bone coverage of Osx $^{+}$ cells and ALP $^{+}$ cells (Fig. 3B). Immunofluorescence analysis showed a significant decrease in the percentage of Osx^{+} cells lining the bone surface on Days 7 ($-13 \pm 5\%$) and 11 ($-25 \pm 7\%$) post ^{223}Ra treatment, which was overcome on Day 18 (Fig. 3B). Interestingly, the amount of perivascular Osx^{+} precursors within the bone marrow significantly increased after 7 days and then decreased over time (Fig. 3C).

No significant change in ALP^{+} cell coverage was detected up to Day 60. However, analysis of the bone interface showed a significant thickening of the ALP $^{+}$ layer on Days 7 and 11 post ^{223}Ra treatment (with a maximum extension of 20.07 ± 7.23 µm from the bone interface towards the bone marrow cavity on Day 7), and significantly decreased by Day 18 (Fig. 3D). Furthermore, as compared to control, the ALP^{+} lining showed an irregular morphology and no colocalization with Osx^{+} signal (Fig. 3D and E).

To assess the degree of osteoblast function and bone mineralization *in vivo* after ^{223}Ra treatment, we measured a dynamic index of bone formation following subsequent injections of two calcium-labeling agents, calcein green and xylenol orange (Fig. 3A and F). We observed no difference in calcium labeling on the femur cortical bone region, consistent with the absence of structural phenotype in this compartment. In the trabecular bone region of the femoral secondary spongiosa, however, the mineral apposition rate (MAR) was significantly decreased in ^{223}Ra-treated mice as compared to the control group (Fig. 3F). Similarly, *in vitro* osteoblast cultures showed significantly decreased calcium deposition upon ^{223}Ra treatment, as monitored by calcein blue staining (Supporting Information Fig. S5). Overall, these results suggest that ^{223}Ra affects osteoblast activity.

3.5. *Effect of ^{223}Ra on osteoclasts in vivo*

To monitor the *in vivo* effects of ^{223}Ra on osteoclasts (bone-resorbing cells), immunofluorescence experiments on bone slices were performed using an anti-tartrate-resistant acid phosphatase (TRAP) antibody. TRAP is an enzyme secreted by osteoclasts and a key effector of their bone resorption activity[31]. Samples were acquired *via* confocal microscopy, and image analysis was performed to quantify the bone coverage of TRAP^{+} cells at different timepoints (Fig. 4A). Image analysis showed a significant, transient increase in TRAP $^{+}$ cell bone coverage 2 days after ^{223}Ra treatment, followed by a significant reduction in TRAP^{+} cells between Days 18 and 40 post treatment, and a recovery on Day 60 (Fig. 4B). These results are in line with results obtained after external beam radiation[20]. Serum analysis of circulating tartrate-resistant acid phosphatase 5b (TRACP5b) confirmed the transient increase in osteoclast number identified by immunofluorescence 2 days post ^{223}Ra treatment and the subsequent drop below baseline (Fig. 4C). Overall, our immunofluorescence analysis coupled with bone turnover serum marker analysis showed a transient osteoclastogenic effect induced by ^{223}Ra, followed by a drop in osteoclast number and activity.

3.6. *Effect of ^{223}Ra on blood vessels in vivo and in vitro*

Next, we investigated the impact of ^{223}Ra on blood vessel biology *in vivo.* Besides delivering oxygen and nutrients within the bone

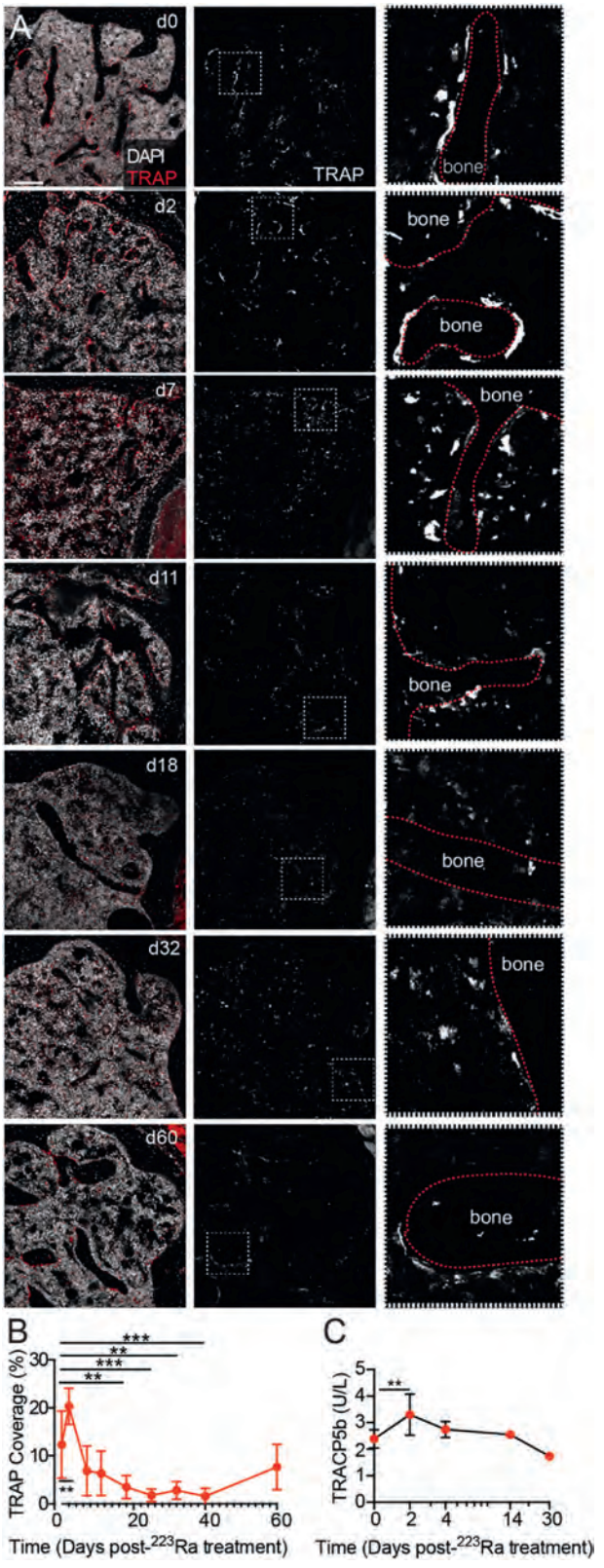

Figure 4 Effect of ^{223}Ra on osteoclasts *in vivo*. (A, B) TRAP^{+} cells, representative images and quantification at different timepoints post ^{223}Ra treatment. Inserts, magnification of TRAP^{+} cell-bone interface. Bar, 100 µm. (C) Serum levels of TRACP5b by ELISA. *P* values by one-way ANOVA with Tukey's HSD *post hoc* test; $P < 0.01$ (**); $P < 0.001$ (***).

marrow compartment, bone blood vessels have been implicated in supporting the function of both the hematopoietic and bone stromal compartments[32]. The density of blood vessels within the bone marrow cavity was assessed by immunofluorescence analysis using an anti-endomucin antibody, a protein expressed in bone sinusoidal blood vessels. Quantitative analysis showed that ^{223}Ra induced a significant, transient increase in the overall amount of bone marrow blood vessels 7 days after treatment, which returned to baseline on Day 11 post treatment (Fig. 5A). Since ^{223}Ra exerts space-dependent cytotoxic effects due to the short penetrance of alpha particles (<100 μm), we further performed a differential analysis of its impact on blood vessels. We selected 4 subregions of the bone marrow, based on their distance from bone, at 0 to 20 (area that showed maximum ALP $^{+}$ positivity upon exposure to ^{223}Ra, see Figs. 3D), 20 to 100, 100 to 200 and > 200 μm. The amount of blood vessels proximal to the bone interface (<20 μm) was significantly reduced 7 days after ^{223}Ra dosing (Fig. 5B), consistent with the transient occupation of this area by ALP^{+} cells (Fig. 5C) but returned to basal levels by Day 11. Vessels at 20 to 100, 100 to 200 and > 200 μm distance, instead, all showed a significant increase on Day 7 (Fig. 5A). In addition, we generated a 3D HUVECs vascular network within a hydrogel system and treated it with 800 Bq/mL ^{223}Ra and monitored the therapy response via live immunofluorescence for up to 2 weeks. No significant difference was identified in GFP signal across the different timepoints between control and treated groups, even initially when radiation was higher, confirming that 3D blood vessel structures are resistant to radiation (Fig. 5D). Additionally,

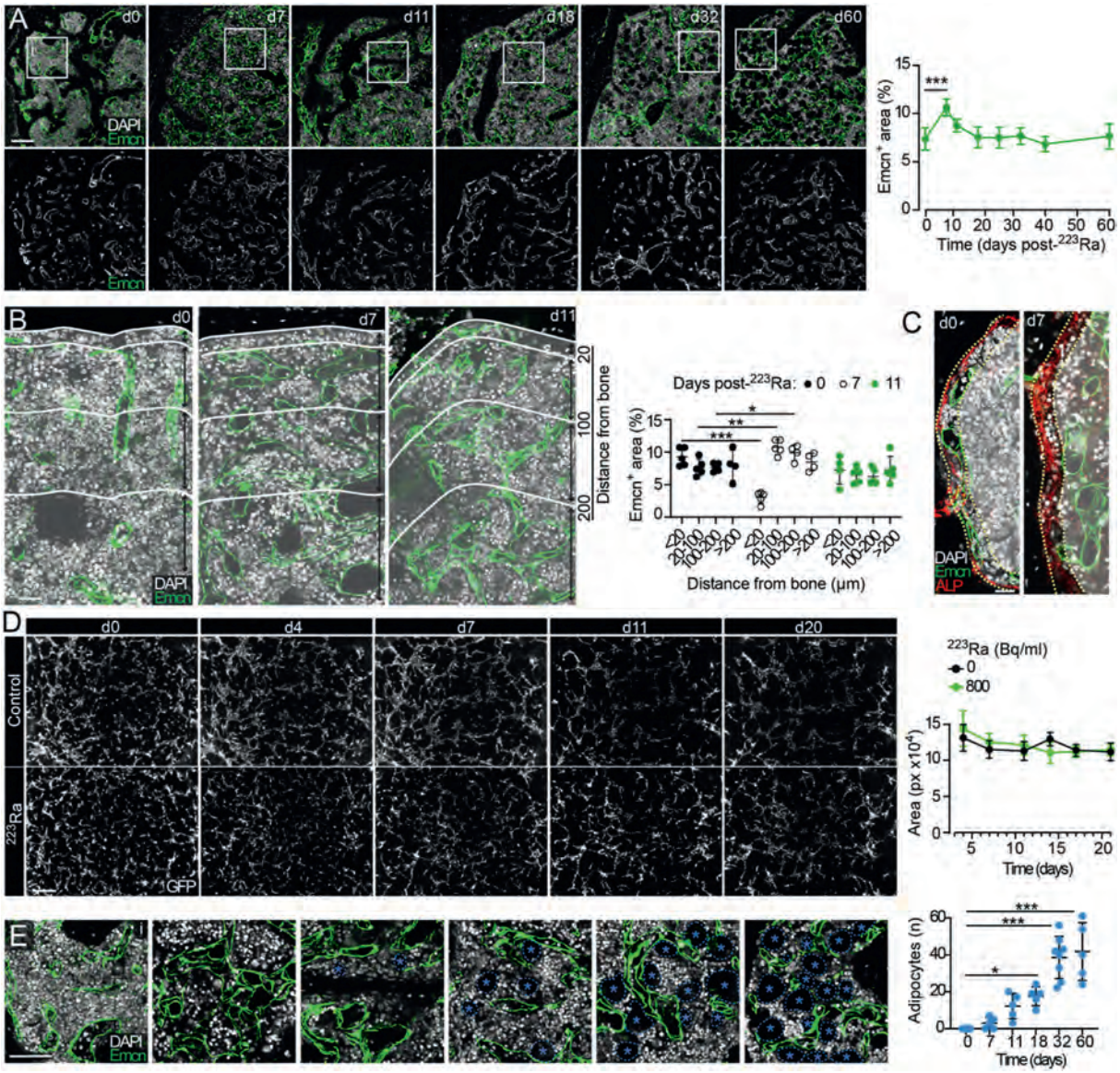

Figure 5 Effects of ^{223}Ra on blood vessels *in vivo* and *in vitro*. (A) Endomucin (emcn), representative images and quantification in tibiae at different timepoints post ^{223}Ra treatment. Box, magnifications shown in (E). Bar, 100 μm. (B) Differential analysis of blood vessel coverage. Bar, 20 μm. (C) Impact of ALP thickening on blood vessel coverage. (D) GFP $^{+}$ HUVEC 3D vascular network treated with different doses of ^{223}Ra, representative images and quantification. Bar, 50 μm. (E) Bone marrow adipocyte infiltration, representative images and quantification. Dashed blue line with asterisk, adipocyte. Bar, 100 μm. *P* values by one-way ANOVA with Tukey's HSD *post hoc* test; $P < 0.05$ (*); $P < 0.01$ (**); $P < 0.001$ (***).

quantification of adipocyte infiltration was performed by counting their number based on their characteristic morphology (a spherical shape and a diameter of >30 μm, distinguishable from endomucin$^+$ blood vessels, characterized by an elongated, irregular shape and frequent interconnections). This morphology-based identification was further validated by adipocyte-specific marker staining and histology (Supporting Information Fig. S6). Results showed a significant increase in adipocyte infiltration 18 days after ^{223}Ra dosing, with a sustained increase up to day 60 (Fig. 5E). Bone marrow adipocyte infiltration is a known effect of ^{223}Ra treatment, as previously shown[33]. Altogether, these data confirm the induction of adipocytes and suggest that ^{223}Ra does not exert major toxic effects on bone blood vessels.

3.7. *Effects of ^{223}Ra+ZA combination treatment on bone properties*

ZA is a drug widely used as bone-protecting agent in patients with bone metastatic cancer and other bone degenerative diseases[34]. ZA has high affinity for hydroxyapatite[35], inhibits osteoclast resorptive activity, and possibly targets other bone stromal cells, including adipocytes and osteoblasts[36-38]. Current clinical guidelines recommend giving ZA to patients receiving ^{223}Ra therapy, as it has been shown to decrease ^{223}Ra-induced bone fragility[39]. However, the biological determinants of this response have never been addressed.

To evaluate the effects of combination ^{223}Ra + ZA treatment on bone microarchitecture, we performed *ex vivo* micro-CT analysis of mouse tibiae harvested 4 weeks post treatment. This analysis showed bone-protective effects of ZA on ^{223}Ra-mouse bones and confirmed our previous findings on trabecular bone damage by ^{223}Ra monotherapy. Specifically, combination ^{223}Ra + ZA prevented a decrease in bone volume fraction and trabecular number (Fig. 6C). Combination treatment also prevented an increase in trabecular separation as compared to ^{223}Ra monotherapy. ZA monotherapy and combination therapy also resulted in a significant increase in trabecular bone thickness. As observed with ^{223}Ra monotherapy, ZA did not induce significant changes in cortical bone thickness (Fig. 6A−C). Taken together, micro-CT data confirmed the deleterious effects of single-agent ^{223}Ra and highlighted the importance of using bone-protecting agents like ZA to prevent radiation-induced trabecular bone damage.

3.8. *Effects of ^{223}Ra + ZA combination treatment in vivo*

To investigate the impact of ZA + ^{223}Ra combination treatment on the bone cellular components, immunofluorescence experiments

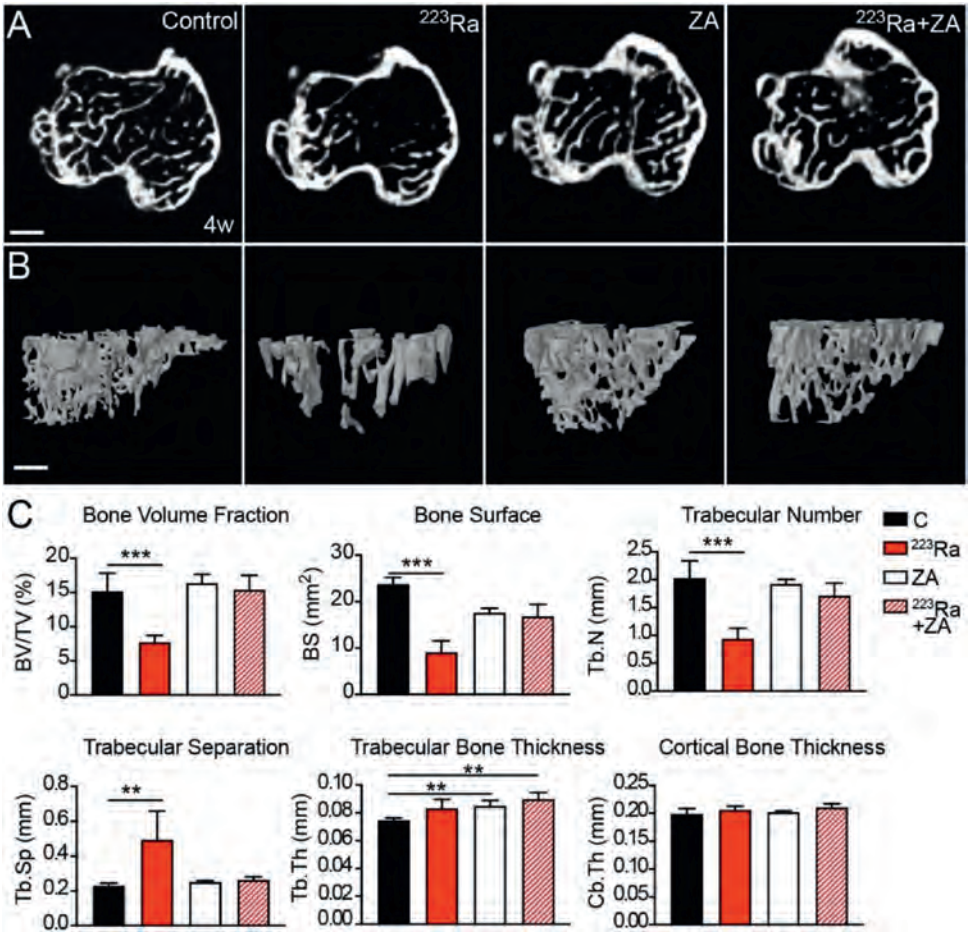

Figure 6 ZA blocks ^{223}Ra-induced deleterious effects on trabecular bone microarchitecture. (A−C) Representative micro-CT images and quantification at 4-week time point. Bar, 300 μm, $n = 4$ tibiae/group. P values by one-way ANOVA with Tukey's HSD *post hoc* test; $P < 0.01$ (**); $P < 0.001$ (***).

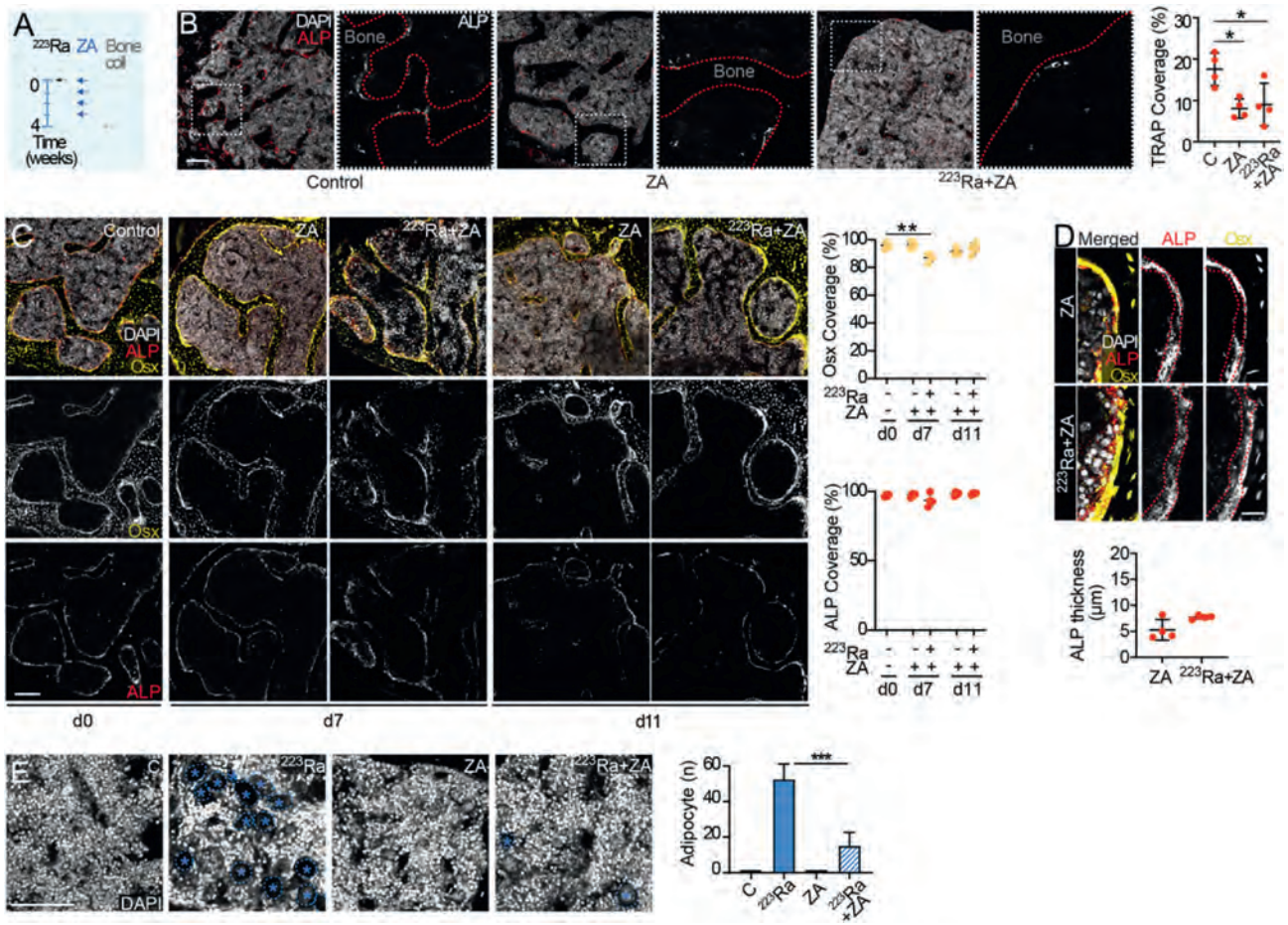

Figure 7 ZA minimizes osteoblast damage and decreases osteoclast number *in vivo*. (A) Experimental design. (B) TRAP^{+} cells, representative images and quantification of tibiae harvested 4 weeks after ZA or ZA + ^{223}Ra treatment. Inserts, magnification of TRAP^{+} cell−bone interface. Bar, 100 μm. (C) Osx and ALP, representative images and quantification in tibiae. Bar, 100 μm. (D) ALP^{+} layer thickness, representative images and quantification. Bar, 30 μm. (E) High magnification inserts (from panel C) and quantification of bone marrow adipocyte infiltration. Dashed blue line with asterisk, adipocyte; Bar, 50 μm. *P* values by one-way ANOVA with Tukey's HSD *post hoc* test; $P < 0.05$ (*); $P < 0.01$ (**); $P < 0.001$ (***).

on bone slices were performed as described above in ^{223}Ra monotherapy experiments. Mice were treated with 1 dose of ^{223}Ra and with ZA weekly, for 4 weeks (Fig. 7A). ZA induced a significant reduction in osteoclast coverage after 4 weeks, with or without ^{223}Ra (Fig. 7B). This is in line with one of the proposed modes of action of ZA, which has been shown to reduce osteoclast number and activity. To determine whether ZA had any impact on the osteoblast population, tibiae from sp7-mcherry mice were harvested at 7 and 11 days post treatment, based on the timing of the Osx $^{+}$ cell reduction observed with ^{223}Ra monotherapy (Fig. 3B). ZA had no effect on Osx^{+} lining cells and did not affect the Osx^{+} cell reduction 7 days post ^{223}Ra treatment ($-9 \pm 3\%$; Fig. 7C); however, ZA completely overcame the major drop in Osx^{+} cells observed 11 days after ^{223}Ra administration ($-25 \pm 7\%$; Fig. 3B). In addition, ZA or combination therapy did not affect ALP bone coverage across the different timepoints. However, when ^{223}Ra was administered in the presence of ZA, the thickening of the ALP^{+} cell layer was not observed (Fig. 7D). Additionally, adipocyte number was quantified 4 weeks post treatment. While ZA treatment alone did not impact adipocyte number (Fig. 7E), when ZA was combined with ^{223}Ra, significantly fewer adipocytes were observed in the bone marrow as compared to ^{223}Ra monotherapy.

Taken together, our findings highlight the importance of using bone-protecting agents to prevent radiation-induced trabecular bone loss and suggest that, besides canonical osteoclast targeting, ZA might improve ^{223}Ra-induced bone fragility by directly or indirectly affecting MSC-derived cell (osteoblasts, adipocytes) biology.

4. Discussion and conclusions

In this study, we investigated the effects of ^{223}Ra on the skeleton and key bone stromal components, including osteoblasts, osteoclasts, blood vessels, and adipocytes. ^{223}Ra therapy had a deleterious effect on the trabecular bone compartment of both long bones (tibiae) and lumbar vertebrae, but not on cortical bone. This may be due to differences in bone composition and remodeling rates between the two compartments, which in turn can affect local incorporation of ^{223}Ra. ^{223}Ra-induced trabecular bone loss was rapid, evident as early as 1 week post treatment, and

resembled age-related osteoporosis[40]. Three-point bending tests did not show major effects of ^{223}Ra on cortical bone mechanical properties, as expected based on our micro-CT data, while m-FEA and simulations of uniaxial compression predicted a significant impact on trabecular mechanical properties. Specifically, stiffness decreased, while deformation, Von Mises stress and strain, and strain energy increased. These computational analyses allowed us to specifically test the mechanical properties of the trabecular region, which would have otherwise been difficult to test *ex vivo* due to the small size of the mouse bones and limited ability to discern the contributions of the cortical versus trabecular compartments to the overall bone mechanical properties.

Collectively, our results showed that ^{223}Ra exerts a major impact on trabecular bone and suggested that vertebrae should be more susceptible to ^{223}Ra-induced bone fragility[41] due to a higher trabecular content as compared to long bones. In further support of these findings, fractures in patients were primarily detected in the spine (66%), followed by the thorax (25%) and pelvis (6%)[14], when whole-body MRI was specifically applied after ^{223}Ra treatment. Long bones, on the other hand, were minimally affected by ^{223}Ra ($\sim$1% of fractures)[14]. Overall, it is possible that the majority of ^{223}Ra-induced fractures are in the spine and are clinically insignificant. This would explain why the ALSYMPCA clinical trial showed no significant increase in bone fractures following treatment with ^{223}Ra (4% in patients receiving ^{223}Ra compared to 5% in those receiving a placebo).

External beam radiation induces trabecular bone loss and other changes in the bone microenvironment through cellular and non-cellular mechanisms[16,20,22]. To determine whether ^{223}Ra inflicted direct, non-cell-mediated bone damage, we performed *ex vivo* micro-CT analysis on bone harvested 2 days post treatment. In the absence of vital cells, ^{223}Ra treatment did not affect bone microarchitecture or trabecular bone volume, suggesting that ^{223}Ra causes changes in the bone microenvironment predominantly by cell-mediated mechanisms rather than through direct damage to the mineralized tissue.

Bone remodeling and homeostasis are closely regulated by the coupled action of osteoblasts and osteoclasts. We first focused on understanding the impact of ^{223}Ra on osteoblasts, the bone-forming component. Immunofluorescence analysis showed a significant decrease in the percentage of Osx $^{+}$ cells lining the bone surface on Days 7 and 11 post ^{223}Ra treatment; however, no significant reduction in ALP^{+} cell coverage was identified up to Day 60. Interestingly, local ALP expression expanded across 2 to 3 layers of Osx^{-} cells in ^{223}Ra-treated mice, likely indicating a perturbation of osteoblast maturation within a few days of ^{223}Ra administration. We identified an increase in perivascular Osx $^{+}$ precursors within the bone marrow 7 days post ^{223}Ra treatment, which decreased to basal levels within 30 days, likely representing osteoprogenitors stimulated by ^{223}Ra-induced damage and involved in repair. As compared to mature osteoblasts, this proliferating cell population might be more efficiently targeted by ^{223}Ra, contributing to the impairment observed in our experiments. We observed no difference in bone formation in cortical bone regions, whereas mineral apposition rate in bone trabeculae was significantly decreased in ^{223}Ra-treated mice as compared to the control group, indicating that ^{223}Ra affected osteoblast bone-forming activity. In addition to partially inducing bone fragility, impaired osteoblast function might explain the reduced osteoblastic activity (circulating ALP levels) observed in patients with PCa and osteoblastic bone metastasis treated with ^{223}Ra[7].

The results of our investigation into the effects of ^{223}Ra on osteoclasts (the bone-resorbing component) showed a transient increase in TRAP $^{+}$ cell bone coverage 2 days after ^{223}Rad treatment, followed by a significant decrease in TRAP $^{+}$ cells by Day 18 post ^{223}Ra treatment, and a recovery of these cells by day 60, in line with published studies involving external beam radiation[20]. The transient spike in osteoclast number was confirmed by serum analysis of TRACP5b, an osteoclast-specific marker. Taken together, these results suggest the trabecular bone loss induced by ^{223}Ra is mediated by a rapid osteoclastic response coupled to dysfunctional bone deposition by osteoblasts.

We also observed a significant increase in adipocyte number as early as 18 days post ^{223}Ra treatment. Adipogenesis and adipocyte infiltration are well-characterized side effects of external radiation, and our data suggest that alpha-particle radiation has a similar effect[42]. Interestingly, bone marrow adipocytes have been shown to negatively control bone mass mediated by bone morphogenetic protein receptor activation[43]. Therefore, increased adipocyte formation might play a role in impaired osteoblast function. As an alternative mechanism, commitment of MSCs toward an adipocyte lineage may further reduce osteoblastogenesis[44].

^{223}Ra induced a significant increase in the overall quantity of bone marrow blood vessels 7 days after treatment, which returned to baseline levels 11 days post treatment. We previously demonstrated that ^{223}Ra has a transient cytotoxic effect on hematopoietic cells, which peaks on Day 4 post treatment, followed by a recovery phase evident on Day 11[33]. Consistently, the loss of hematopoietic cells in response to external beam radiation triggers vessel dilation, permeability, and endothelial cell proliferation[45]. Additionally, our differential analysis showed that the amount of blood vessels proximal to the bone interface ($<$20 μm; the same area affected by ALP thickening) was significantly reduced at 7 days after ^{223}Ra dosing but returned to baseline levels on Day 11. *In vitro* experiments with 3D vascular networks did not show any ^{223}Ra-mediated reduction of these vascular structures, suggesting that ^{223}Ra does not exert direct toxicity on blood vessels.

ZA is commonly used as a bone-protecting agent in the clinical setting, and its administration to ^{223}Ra patients showed positive effects on bone fragility[24]. Our results confirmed the bone-protective properties of ZA on the trabecular bone damage induced by ^{223}Ra, likely via its inhibitory effect on bone resorption. Interestingly, ZA significantly decreased ^{223}Ra-induced bone marrow adipocyte density, loss of Osx^{+} cells, and impact on ALP expression; it remains to be determined whether this occurs via direct action on MSCs, osteoblasts, or adipocytes or as an indirect effect secondary to reduced bone turnover. Nevertheless, these results confirm the importance of using ZA in combination with ^{223}Ra therapy to prevent trabecular bone loss and reduce the overall impact of ^{223}Ra on the bone cell population, as recommended by all major medical guidelines. Comparison with other anti-resorptive agents with convergent and divergent mechanisms of action (*i.e.*, denosumab, which inhibits osteoclast maturation) is needed to identify the best option to rationally prevent ^{223}Ra-induced bone fragility.

Acknowledgments

This work was supported by Bayer HealthCare Pharmaceuticals Inc. (57440); Department of Defense, CDMRP-KCRP (KC210132P1, USA); University of Texas MD Anderson Cancer

Center; Cancer Prevention and Research Institute of Texas (RP230160, USA); National Institutes of Health (P41EB023833; P30CA016672, USA). We thank Dr. Ralph Adams (Max Planck Institute for Molecular Biomedicine, Münster, Germany) for sharing mCherry-Sp7 (Osx^{+}) mice. We thank Sarah Townsend (University of Texas MD Anderson Cancer Center, TX, USA) for careful editing of our paper.

Author contributions

Sergio Barrios, Elisa Serafini, Nicholas J. Dunbar, Paul Corn, Florent Elefteriou, Catherine Ambrose, Stefano Casarin, Antonio G. Mikos, Eleonora Dondossola designed the research. Sergio Barrios, Elisa Serafini, Ludovica La Posta, D. Nicole Meyers, Eleonora Dondossola carried out the experiments and performed data analysis. Nicholas J. Dunbar, Florent Elefteriou, Catherine G. Ambrose, Stefano Casarin participated part of the experiments. Sergio Barrios, Elisa Serafini, Stefano Casarin, Antonios G. Mikos, and Eleonora Dondossola wrote the manuscript. Ludovica La Posta, D. Nicole Meyers, Nicholas J. Dunbar, Paul G. Corn, Florent Elefteriou, Catherine G. Ambrose revised the manuscript. All the authors have read and approved the final manuscript.

Conflicts of interest

No potential conflicts of interest relevant to this article exist. The funders had no role in the design of the study, the collection/analysis/interpretation of data, or the decision to submit the manuscript.

Appendix A. Supporting information

Supporting information to this article can be found online at https://doi.org/10.1016/j.apsb.2025.07.035.

References

1. Torre LA, Bray F, Siegel RL, Ferlay J, Lortet-Tieulent J, Jemal A. Global cancer statistics, 2012. *CA Cancer J Clin* 2015;**65**:87−108.
2. Weilbaecher KN, Guise TA, McCauley LK. Cancer to bone: a fatal attraction. *Nat Rev Cancer* 2011;**11**:411−25.
3. Croucher PI, McDonald MM, Martin TJ. Bone metastasis: the importance of the neighbourhood. *Nat Rev Cancer* 2016;**16**:373−86.
4. Woodward E, Jagdev S, McParland L, Clark K, Gregory W, Newsham A, et al. Skeletal complications and survival in renal cancer patients with bone metastases. *Bone* 2011;**48**:160−6.
5. Yuasa T, Urakami S, Yamamoto S, Yonese J, Saito K, Takahashi S, et al. Treatment outcome and prognostic factors in renal cell cancer patients with bone metastasis. *Clin Exp Metastasis* 2011;**28**:405−11.
6. Abou DS, Ulmert D, Doucet M, Hobbs RF, Riddle RC, Thorek DL. Whole-body and microenvironmental localization of radium-223 in naive and mouse models of prostate cancer metastasis. *J Natl Cancer Inst* 2016;**108** [页码].
7. Parker C, Nilsson S, Heinrich D, Helle SI, O'Sullivan JM, Fossa SD, et al. Alpha emitter radium-223 and survival in metastatic prostate cancer. *N Engl J Med* 2013;**369**:213−23.
8. Bruland OS, Nilsson S, Fisher DR, Larsen RH. High-linear energy transfer irradiation targeted to skeletal metastases by the alpha-emitter 223Ra: adjuvant or alternative to conventional modalities?. *Clin Cancer Res* 2006;**12**. 6250s-7s.
9. Dondossola E, Casarin S, Paindelli C, De-Juan-Pardo EM, Hutmacher DW, Logothetis CJ, et al. Radium 223-mediated zonal cytotoxicity of prostate cancer in bone. *J Natl Cancer Inst* 2019;**111**: 1042−50.
10. Sartor O, Coleman R, Nilsson S, Heinrich D, Helle SI, O'Sullivan JM, et al. Effect of radium-223 dichloride on symptomatic skeletal events in patients with castration-resistant prostate cancer and bone metastases: results from a phase 3, double-blind, randomised trial. *Lancet Oncol* 2014;**15**:738−46.
11. Suominen MI, Rissanen JP, Kakonen R, Fagerlund KM, Alhoniemi E, Mumberg D, et al. Survival benefit with radium-223 dichloride in a mouse model of breast cancer bone metastasis. *J Natl Cancer Inst* 2013;**105**:908−16.
12. Ueno NT, Tahara RK, Fujii T, Reuben JM, Gao H, Saigal B, et al. Phase II study of Radium-223 dichloride combined with hormonal therapy for hormone receptor-positive, bone-dominant metastatic breast cancer. *Cancer Med* 2020;**9**:1025−32.
13. Morris MJ, Corey E, Guise TA, Gulley JL, Kevin Kelly W, Quinn DI, et al. Radium-223 mechanism of action: implications for use in treatment combinations. *Nat Rev Urol* 2019;**16**:745−56.
14. Hijab A, Curcean S, Tunariu N, Tovey H, Alonzi R, Staffurth J, et al. Fracture risk in men with metastatic prostate cancer treated with radium-223. *Clin Genitourin Cancer* 2021;**19**:e299−305.
15. Suominen MI, Fagerlund KM, Rissanen JP, Konkol YM, Morko JP, Peng Z, et al. Radium-223 inhibits osseous prostate cancer growth by dual targeting of cancer cells and bone microenvironment in mouse models. *Clin Cancer Res* 2017;**23**:4335−46.
16. Green DE, Rubin CT. Consequences of irradiation on bone and marrow phenotypes, and its relation to disruption of hematopoietic precursors. *Bone* 2014;**63**:87−94.
17. Oest ME, Policastro CG, Mann KA, Zimmerman ND, Damron TA. Longitudinal effects of single hindlimb radiation therapy on bone strength and morphology at local and contralateral sites. *J Bone Miner Res* 2018;**33**:99−112.
18. Costa S, Reagan MR. Therapeutic irradiation: consequences for bone and bone marrow adipose tissue. *Front Endocrinol* 2019;**10**:587.
19. Zhang J, Qiu X, Xi K, Hu W, Pei H, Nie J, et al. Therapeutic ionizing radiation induced bone loss: a review of *in vivo* and *in vitro* findings. *Connect Tissue Res* 2018;**59**:509−22.
20. Green DE, Adler BJ, Chan ME, Lennon JJ, Acerbo AS, Miller LM, et al. Altered composition of bone as triggered by irradiation facilitates the rapid erosion of the matrix by both cellular and physicochemical processes. *PLoS One* 2013;**8**:e64952.
21. Bartlow CM, Mann KA, Damron TA, Oest ME. Altered mechanical behavior of demineralized bone following therapeutic radiation. *J Orthop Res* 2021;**39**:750−60.
22. Green DE, Adler BJ, Chan ME, Rubin CT. Devastation of adult stem cell pools by irradiation precedes collapse of trabecular bone quality and quantity. *J Bone Miner Res* 2012;**27**:749−59.
23. Chandra A, Wang L, Young T, Zhong L, Tseng WJ, Levine MA, et al. Proteasome inhibitor bortezomib is a novel therapeutic agent for focal radiation-induced osteoporosis. *FASEB J* 2018;**32**:52−62.
24. Gillessen S, Choudhury A, Rodriguez-Vida A, Nole F, Diaz EG, Roumeguere TA, et al. Decreased fracture rate by mandating bone protecting agents in the EORTC 1333/PEACEIII trial combining Ra223 with enzalutamide versus enzalutamide alone: an updated safety analysis. *J Clin Oncol* 2021;**39**:5002.
25. Parr W, Chamoli U, Jones A, Walsh W, Wroe S. Finite element micro-modelling of a human ankle bone reveals the importance of the trabecular network to mechanical performance: new methods for the generation and comparison of 3D models. *J Biomech* 2013;**46**: 200−5.
26. Bevill G, Keaveny TM. Trabecular bone strength predictions using finite element analysis of micro-scale images at limited spatial resolution. *Bone* 2009;**44**:579−84.
27. Oftadeh R, Perez-Viloria M, Villa-Camacho JC, Vaziri A, Nazarian A. Biomechanics and mechanobiology of trabecular bone: a review. *J Biomech Eng* 2015;**137**:108021−1080215.
28. Sinha KM, Zhou X. Genetic and molecular control of osterix in skeletal formation. *J Cell Biochem* 2013;**114**:975−84.

29. Yeniyol S, Ricci JL. Alkaline phosphatase levels of murine pre-osteoblastic cells on anodized and annealed titanium surfaces. *Eur Oral Res* 2018;**52**:12−9.
30. Schindelin J, Arganda-Carreras I, Frise E, Kaynig V, Longair M, Pietzsch T, et al. Fiji: an open-source platform for biological-image analysis. *Nat Methods* 2012;**9**:676−82.
31. Blumer MJ, Hausott B, Schwarzer C, Hayman AR, Stempel J, Fritsch H. Role of tartrate-resistant acid phosphatase (TRAP) in long bone development. *Mech Dev* 2012;**129**:162−76.
32. Hendriks M, Ramasamy SK. Blood vessels and vascular niches in bone development and physiological remodeling. *Front Cell Dev Biol* 2020;**8** [页码].
33. Parlani M, Boccalatte F, Yeaton A, Wang F, Zhang J, Aifantis I, et al. (223)Ra induces transient functional bone marrow toxicity. *J Nucl Med* 2022;**63**:1544−50.
34. Polascik TJ, Mouraviev V. Zoledronic acid in the management of metastatic bone disease. *Therapeut Clin Risk Manag* 2008;**4**:261−8.
35. Saad F, Gleason DM, Murray R, Tchekmedyian S, Venner P, Lacombe L, et al. Long-term efficacy of zoledronic acid for the prevention of skeletal complications in patients with metastatic hormone-refractory prostate cancer. *J Natl Cancer Inst* 2004;**96**: 879−82.
36. Jin J, Wang L, Wang X-k, Lai P-l, Huang M-j, Jin D-d, et al. Risedronate inhibits bone marrow mesenchymal stem cell adipogenesis and switches RANKL/OPG ratio to impair osteoclast differentiation. *J Surg Res* 2013;**180**:e21−9.
37. Oryan A, Sahvieh S. Effects of bisphosphonates on osteoporosis: focus on zoledronate. *Life Sci* 2021;**264**:118681.
38. Maruotti N, Corrado A, Neve A, Cantatore FP. Bisphosphonates: effects on osteoblast. *Eur J Clin Pharmacol* 2012;**68**:1013−8.
39. Cheer SM, Noble S. Zoledronic acid. *Drugs* 2001;**61**:799−805.
40. Shim J, Iwaya C, Ambrose CG, Suzuki A, Iwata J. Micro-computed tomography assessment of bone structure in aging mice. *Sci Rep* 2022; **12**:8117.
41. Osterhoff G, Morgan EF, Shefelbine SJ, Karim L, McNamara LM, Augat P. Bone mechanical properties and changes with osteoporosis. *Injury* 2016;**47**(Suppl 2):S11−20.
42. Zou Q, Hong W, Zhou Y, Ding Q, Wang J, Jin W, et al. Bone marrow stem cell dysfunction in radiation-induced abscopal bone loss. *J Orthop Surg Res* 2016;**11**:3.
43. Zou W, Rohatgi N, Brestoff JR, Li Y, Barve RA, Tycksen E, et al. Ablation of fat cells in adult mice induces massive bone gain. *Cell Metab* 2020;**32**. 801-13.e6.
44. Muruganandan S, Govindarajan R, Sinal CJ. Bone marrow adipose tissue and skeletal health. *Curr Osteoporos Rep* 2018;**16**:434−42.
45. Chen Q, Liu Y, Jeong H-W, Stehling M, Dinh VV, Zhou B, et al. Apelin+ endothelial niche cells control hematopoiesis and mediate vascular regeneration after myeloablative injury. *Cell Stem Cell* 2019;**25**. 768-83.e6.